*J. Fluid Mech.* (1993), *vol.* 246, *pp.* 143–161



# On the response of a reservoir sidearm to diurnal heating and cooling

By D. E. FARROW† AND J. C. PATTERSON

Centre for Water Research, University of Western Australia, Nedlands, WA 6009, Australia

(Received 21 November 1991 and in revised form 22 June 1992)

During the day, the shallower regions of a reservoir sidearm absorb more heat per unit volume than the deeper parts, leading to a horizontal pressure gradient that drives a circulation in the sidearm. At night, the shallow regions cool more rapidly, leading to a circulation in the opposite direction. Since the spin-up time of a typical sidearm is at least of the same order as a day, the flow within a diurnally forced sidearm is principally an inertia–buoyancy balance. In this paper, a diurnally forced sidearm is modelled by periodically forced natural convection in a triangular cavity. The periodic forcing enters the model via an internal heating/cooling term in the temperature equation. Reservoir sidearms typically have small bottom slopes and this fact can be exploited to obtain asymptotic solutions of the resulting equations. These solutions clearly demonstrate the transition from the viscous-dominated flow in the shallows to the inertia-dominated flow in the deeper parts. In the inertia-dominated region, the flow response significantly lags the forcing. Numerical solutions of the full nonlinear problem are consistent with the asymptotic solutions.

## 1. Introduction

The understanding of the fluid mechanics of lakes and reservoirs has expanded rapidly in recent years owing to the importance of fluid dynamical processes for determining the quality of water supply. A recent review of dynamical processes pertinent to lakes and reservoirs can be found in Imberger & Patterson (1990). In particular, processes that give rise to horizontal rather than vertical transport of water properties have received considerable recent attention. An example of a limnological situation where horizontal processes play a part in the overall dynamics is differential heating or cooling which occurs when neighbouring regions of the same water body are heated or cooled relative to each other. This leads to a horizontal pressure gradient due to thermal expansion that can drive a significant flow. The flooding of a reservoir basin usually involves the inundation of many small valleys around its perimeter. These flooded valleys (which are then called sidearms) are typically only tens to hundreds of metres long and only a few metres deep where they join the main body of the reservoir. Sidearms are often well protected from the wind and so thermal forcing associated with heating and cooling is an important mechanism for promoting exchange of water between the sidearm and the main body of the reservoir.

During the day, the water column absorbs solar radiation according to Beer's law (see, for example, Kirk 1986); the intensity of the light decays exponentially with depth and the rate of decay is a function of the wavelength of the light and the

† Present address: Department of Applied Mathematics, University of Adelaide, Adelaide SA 5001, Australia.

turbidity of the water. This leads to a shallow surface layer that can be several degrees warmer than the underlying water. Near the shore, topographic effects become important as the heat absorbed is distributed over a decreasing depth and the water in the shallows becomes, on average, warmer than the deeper offshore regions. As pointed out by Monismith, Imberger & Morrison (1990), this heating mechanism leads to the temperature scaling with the inverse of the distance from the shore. This temperature structure drives a surface outflow of warm water from the edges of a reservoir sidearm. Flows due to this mechanism have been observed by Adams & Wells (1984) and Monismith *et al.* (1990) with measured velocities of the order of 5 cm $s^{-1}$. These studies also indicated that the three-dimensional topography of a reservoir sidearm leads to a complicated three-dimensional velocity and temperature structure.

At night, surface cooling leads to a circulation in the opposite direction. Surface cooling destabilizes the surface waters that have been stabilized during the day, leading to a deeper surface mixed layer. This mixed layer is approximately isothermal except near the edges of the sidearm where the local depth is less than that of the mixed layer. In this region, heat loss occurs approximately uniformly over the local depth but at a greater volumetric rate as the depth decreases since an approximately constant surface flux is distributed over a decreasing depth. The cooler water at the edges of the sidearm travels under gravity down the sloping bottom away from the boundaries, setting up a circulation in the opposite direction to the daytime circulation.

In the absence of wind or other momentum inputs, the flows described above can be classified as natural convection, for which there is a large body of literature. Natural convection in shallow cavities is the aspect most relevant to the geophysical phenomena considered in this paper.

Sturm (1981) and Jain (1982) studied a cooling pond sidearm and their studies are relevant to the present situation. In those papers, steady-state integral solutions for heat and mass fluxes in idealized cooling pond sidearms were found which are consistent with the experimental results of Brocard & Harleman (1980). Poulikakos & Bejan (1983) found the steady-state flow and temperature structure in an attic space with a horizontal bottom and an arbitrarily shaped heated upper boundary using asymptotic methods. In more directly geophysically motivated studies, Scott & Imberger (1988) and Scott (1988) considered the steady-state flow in three-dimensional cavities of arbitrary geometry which were used to model estuarine dynamics. Those studies considered the steady-state density and flow structures in two- and three-dimensional estuaries subject to a number of buoyancy and momentum inputs, again using asymptotic methods.

All this work has been for steady-state conditions. However, Monismith *et al.* (1990) show that the spin-up time for a typical sidearm is at least of the same order as the period of the diurnal forcing which means that, at least in the deeper parts of a sidearm, steady state is not achieved within one period of the diurnal cycle. This was confirmed by the observations of Monismith *et al.* where the night-time flow in the sidearm did not reverse until about seven hours after the heat flux at the surface had changed from cooling to heating. Consequently, the flow is intrinsically unsteady and the transient behaviour must also be included in a model of sidearm behaviour, at least for the diurnally forced case.

Patterson (1984) studied transient natural convection in an internally heated rectangular cavity which was initially isothermal and at rest. he found that the approach to steady state could be classified as either conductive, transitional or

convective depending on the value of the Grashof number $Gr$ relative to combinations of the aspect ratio of the cavity and the Prandtl number $\sigma = \nu/\kappa$ of the fluid, where

$$Gr = g\alpha \Delta T h^3/\nu^2. \tag{1}$$

In (1) and the definition of $\sigma$, $g$ is the acceleration due to gravity, $\alpha$ is the thermal expansion coefficient, $\Delta T = Q_0 hl^3/\nu$ where $Q_0$ is the magnitude of the volumetric heating rate, $l$ is the length of the cavity, $h$ is the height of the cavity, $\nu$ is the kinematic viscosity and $\kappa$ is the thermal diffusivity. The classifications could be further divided into sub-classifications characterized by the relative magnitude of various timescales of the flow and the nature of the internal balances at steady state. In some cases, the approach to steady state was oscillatory, but in all cases it was achieved in a timescale of $h^2/\nu$ which is just the time it takes for viscosity to diffuse momentum across the depth of the cavity. For a reservoir sidearm, $h$ is typically 5 m, leading to a spin-up time of $\sim 2.5 \times 10^7$ s ($\approx 250$ days) for molecular viscosity or $\sim 2.5 \times 10^5$ s ($\approx 2.5$ days) for a typical value of the eddy viscosity of $10^{-4}$ m$^2$ s$^{-1}$. Thus, even if the flow is turbulent, the spin-up time is comparable to the timescale of the forcing and so, as already discussed, the flow in a typical sidearm is intrinsically unsteady.

There are very few analytical or experimental studies aimed at understanding the transient response of a cavity with sidearm geometry to thermal forcing. Patterson (1987) numerically investigated the daytime circulation, assuming that the heat input was uniformly distributed over the local depth in a triangular cavity. Further assuming that the bottom of the model sidearm was perfectly reflective and the bottom slope was small led to a horizontally linear internal heating source term. An additional feature of this model was an adjustment of the mean heat input so the system would reach steady state. The results of Patterson (1987) show that even though the internal heating is vertically uniform, advection ultimately sets up a strong stratification with horizontal isotherms in the majority of the cavity and vertical isotherms occurring only in the shallow tip region.

Horsh & Stefan (1988) numerically studied the night-time cooling phase in a triangular cavity with a fixed heat flux at the surface. They found that the flow initially consisted of a number of recirculating regions associated with sinking plumes of cooled surface water. At the same time, a gravity current of cold water emerged from the tip and flowed down the sloping bottom in much the same manner as the currents observed by Monismith *et al.* (1990). After a sufficiently long time, the gravity current ejected from the tip travelled the length of the flow domain and Horsh & Stefan found that the recirculating regions coalesced as the gravity current began to dominate the flow, ultimately leading to a single cell occupying the entire cavity.

Despite the fact that the spin-up time for flow in a sidearm is of the same order as the period of the forcing, there appear to be no analytical or experimental studies of periodically forced natural convection in sidearm geometries. In the sidearm case, the interaction between the timescales of the forcing and the timescales of the response is of primary interest. The observations of Monismith *et al.* (1990) show that the flow in a sidearm can significantly lag the forcing. The factors that determine this lag and the influence it has on the flow structure within the sidearm are issues that will be examined in this paper.

## 2. Model formulation

The flow in a reservoir sidearm is modelled by the two-dimensional flow of a fluid contained in the infinite wedge $0 < z' < -Ax'$, where $x'$ is the horizontal coordinate measured from the tip and $z'$ is the vertical coordinate measured positive upwards from the upper boundary. Figure 1 shows the geometry of the flow domain. This flow domain is the simplest possible that allows for a non-uniform depth. Although Poulikakos & Bejan (1983) discuss the influence of a more general geometry in their discussion of the fluid mechanics of an attic space, their solution is for the steady-state problem with different boundary conditions and is not applicable here. In that paper, $z' = -Ax'$ is replaced by $z' = -Af(x')$. However, as $A \to 0$ only $f(x')$ and $\mathrm{d}f(x')/\mathrm{d}x'$ affect the flow. Specifically, $f(x')$ and $\mathrm{d}f(x')/\mathrm{d}x'$ only affect the magnitude of the local horizontal pressure gradient (Poulikakos & Bejan 1983). Hence in this paper, where only the $A \to 0$ equations are solved, there is little to gain by having a more general bottom shape.

Temperature differences in reservoir sidearms are typically small and so the Boussinesq approximation for the density is appropriate. The diurnal forcing of the flow is modelled by an internal heating and cooling term included in the temperature equation. This term is formulated by distributing a surface heat flux of $I = I_0 \cos(2\pi t'/P)$ $\mathrm{Wm}^{-2}$ (where $I_0$ is the maximum heat flux, $t'$ is time and $P$ is the period of one day) uniformly over the local depth. This leads to a heat source/sink term in the temperature equation of the form

$$Q(x', t') = \frac{I_0}{\rho_0 C_p A x'} \cos(2\pi t'/P)\ ^{\circ}\mathrm{C\ s}^{-1}. \tag{2}$$

The $Ax'$ that appears in the denominator of $Q$ is just the local depth over which the heat flux has been distributed. In (2), $\rho_0$ is the reference density and $C_p$ is the specific heat of water. The magnitude of $Q$ increases towards $x' = 0$. This will give rise to larger temperature gradients there, consistent with field observations. The restriction to a vertically uniform heating/cooling term in this model is a significant simplification of the somewhat more complex heat input/output mechanisms operating in a real sidearm. The model formulated in this paper is expected to be relevant in the near-shore region where topography dominates. A more sophisticated model for the thermal forcing would considerably complicate subsequent analysis and involve extra parameters characterizing the type of forcing. It is for these reasons that this work is restricted to a vertically uniform thermal forcing.

The non-dimensionalization of the resulting system of equations proceeds as follows. There is a clear timescale for the flow given by $P$, the period of the forcing. The assumed geometry of the flow domain imposes no natural lengthscale but there is a vertical lengthscale $(\nu P)^{\frac{1}{2}}$ where $\nu$ is the viscosity of the water which, for simplicity, is assumed to be constant. This lengthscale is just the distance over which viscosity is able to act within one period of the forcing. This is the fundamental lengthscale of the flow and it is used to non-dimensionalize the vertical coordinate. The geometry of the flow domain then imposes a horizontal lengthscale $A^{-1}(\nu P)^{\frac{1}{2}}$. Balancing the unsteady term in the temperature equation with the internal heating/cooling term gives rise to a temperature perturbation scale of $I_0 P/(\rho_0 C_p (\nu P)^{\frac{1}{2}})$. A balance between the vertical pressure gradient and buoyancy yields a scale for the pressure which when balanced with horizontal shear yields the horizontal velocity scale $Ag\alpha I_0 P^2/(\rho_0 C_p (\nu P)^{\frac{1}{2}})$, where $\alpha$ is the coefficient of thermal expansion. Finally, the continuity equation yields a vertical velocity scale

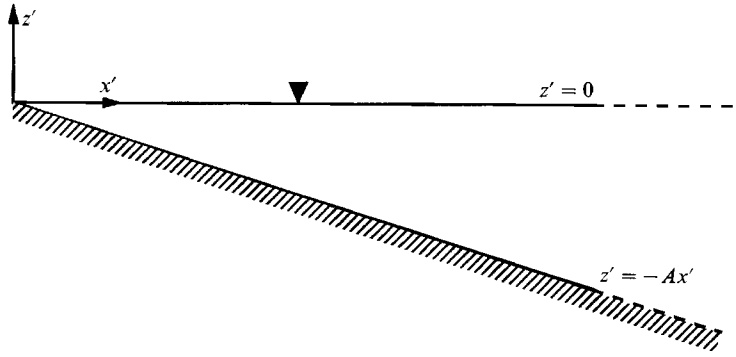


FIGURE 1. Sketch of the geometry of the flow domain showing the origin of the coordinate system at the tip of the wedge.

$A^2 g\alpha I_0 P^2/(\rho_0 P_p (\nu P)^{\frac{1}{2}})$. Introducing a non-dimensional stream function $\psi$ yields the conservation of vorticity and heat equations

$$\psi_{tzz}+A^2\psi_{txx}+A^2Gr(\psi_x\psi_{zzz}-\psi_z\psi_{zzx}+A^2(\psi_x\psi_{xxz}-\psi_z\psi_{xxx})) = \psi_{zzzz}+2A^2\psi_{xxzz}+A^4\psi_{xxxx}+T_x, \quad (3)$$

and
$$\partial T/\partial t+A^2Gr(-\psi_z T_x+\psi_x T_z) = (A^2T_{xx}+T_{zz})/\sigma+\cos(2\pi t)/x, \quad (4)$$

with the boundary conditions

$$\psi = \psi_{zz} = 0, \quad T_z = 0 \quad \text{on} \quad z = 0, \quad (5)$$

$$\psi = \psi_z = 0, \quad (T_z+A^2T_x)/(1+A^2)^{\frac{1}{2}} = 0, \quad \text{on} \quad z = -x, \quad (6)$$

and the initial conditions $\psi = T = 0$ at $t = 0$ where $u = -\psi_z$, $w = \psi_x$ and all variables are now non-dimensional, and the non-dimensional parameters for the problem are the bottom slope $A$, the Prandtl number $\sigma = \nu/\kappa$ and $Gr$ the Grashof number which is now given by

$$Gr = \frac{g\alpha I_0 P^2}{\rho_0 C_p \nu}.$$

The boundary conditions (5) and (6) arise from the assumptions that the upper surface $z = 0$ is not deformed and is stress free, the sloping bottom boundary is rigid and that all heat input/output in the system is included in the internal source/sink term in (4). This last assumption leads to all boundaries being insulated. The system of equations (3)–(6) is unsteady and nonlinear making a full analytical solution difficult to obtain. In the next section, asymptotic solutions for the temperature and velocity fields are found as the bottom slope $A$ becomes small.

## 3. Asymptotic solution

The small parameter $A$ appears as even powers in the boundary-value problem (3)–(6). Following Cormack, Leal & Imberger (1974), the dependent variables are expanded as a series in $A^2$:

$$T = T^{(0)}+A^2T^{(2)}+A^4T^{(4)}+\ldots, \qquad \psi = \psi^{(0)}+A^2\psi^{(2)}+A^4\psi^{(4)}+\ldots. \quad (7)$$

Substituting these expressions into (3) and (4) and equating like powers of $A$ yields

a system of linear partial differential equations that can, in principle, be solved recursively. The general $O(A^n)$ equations are ($n$ even)

$$\psi_{tzz}^{(n)}+\psi_{txx}^{(n-2)}+Gr\sum_{\substack{k=0\\ k\text{ even}}}^{n-2}[\psi_x^{(k)}\psi_{zzz}^{(n-k-2)}-\psi_z^{(k)}\psi_{zzx}^{(n-k-2)}]$$
$$+Gr\sum_{\substack{k=0\\ k\text{ even}}}^{n-4}[\psi_x^{(k)}\psi_{xxz}^{(n-k-4)}-\psi_z^{(k)}\psi_{xxx}^{(n-k-4)}]=\psi_{zzzz}^{(n)}+2\psi_{xxzz}^{(n-2)}+\psi_{xxxx}^{(n-4)}+T_x^{(n)} \quad (8)$$

and

$$T_t^{(n)}+Gr\sum_{\substack{k=0\\ k\text{ even}}}^{n-2}[-\psi_z^{(k)}T_x^{(n-k-2)}+\psi_x^{(k)}T_z^{(n-k-2)}]=\frac{1}{\sigma}(T_{zz}^{(n)}+T_{xx}^{(n-2)})+\delta_{n0}\cos(2\pi t)/x \quad (9)$$

with boundary conditions

$$\left.\begin{aligned}\psi^{(n)}=\psi_{zz}^{(n)}=0,\quad T_z^{(n)}=0\quad\text{on}\quad z=0,\\ \psi^{(n)}=\psi_z^{(n)}=0\quad\text{on}\quad z=-x,\\ T_z^{(n)}+\sum_{\substack{k=2\\ k\text{ even}}}^{n}(-1)^{k/2}\frac{1.3\ldots(k-1)}{2.4\ldots k}(T_z^{(n-k)}+T_x^{(n-k-2)})=0\quad\text{on}\quad z=-x,\end{aligned}\right\} \quad (10)$$

and initial conditions

$$\psi^{(n)}=T^{(n)}=0\quad\text{at}\quad t=0 \quad (11)$$

where quantities with negative superscripts are zero.

Only the $O(A^0)$ equations are solved here and these are

$$\psi_{tzz}^{(0)}=\psi_{zzzz}^{(0)}+T_x^{(0)}, \quad (12)$$

$$T_t^{(0)}=T_{zz}^{(0)}/\sigma+\cos(2\pi t)/x \quad (13)$$

with boundary conditions

$$\psi^{(0)}=\psi_{zz}^{(0)}=0,\quad T_z^{(0)}=0\quad\text{on}\quad z=0, \quad (14)$$

$$\psi^{(0)}=\psi_z^{(0)}=0,\quad T_z^{(0)}=0\quad\text{on}\quad z=-x, \quad (15)$$

and the initial conditions

$$\psi^{(0)}=T^{(0)}=0\quad\text{at}\quad t=0. \quad (16)$$

Thus, at zero order, the flow is set up in the following way. The fluid in the cavity is differentially heated or cooled. This leads to a pressure field that drives a gentle circulation. So gentle, in fact, that the background temperature field and the resulting circulation are decoupled. The question of the validity of these asymptotic equations is addressed later.

From (13), $T^{(0)}$ can be obtained by direct integration to give

$$T^{(0)}=\sin(2\pi t)/2\pi x. \quad (17)$$

Thus, as mentioned earlier, the main balance as $A\to 0$ is between the internal source and the unsteady term. Because of this and the fact that horizontal conduction is an $O(A^2)$ effect, the temperature is independent of the Prandtl number $\sigma$. This temperature structure varies with time representing the change in sign of the horizontal gradient from day to night. The zero-order temperature solution (17) is very simple but it still has some of the desired features that make it consistent with observed sidearm temperature fields. In particular, the magnitude of the horizontal gradient and $T^{(0)}$ increases as $x\to 0$.

Recall that the temperature source term in the zero-order temperature equation (13) is $\cos(2\pi t)/x$ so the temperature (17) lags the forcing by one quarter of a period. This corresponds to 6 hours in the diurnal cycle. In other words, the horizontal temperature gradient in a typical sidearm will not reverse until about 6 hours after the net heat transfer into or out of the sidearm has changed sign.

Substituting for the horizontal temperature gradient yields the equation for $\psi^{(0)}$

$$\psi^{(0)}_{tzz} = \psi^{(0)}_{zzzz} - \sin(2\pi t)/2\pi x^2 \tag{18}$$

with the boundary conditions (14) and (15).

The solution can be found by taking Laplace transforms in $t$, the details of which are not included here. The solution for the horizontal velocity $u^{(0)} = -\partial\psi^{(0)}/\partial z$ is given by

$$\begin{aligned} u^{(0)}(x,z,t) = {} & \overbrace{-\frac{1}{96\pi x^2}\sin(2\pi t)(z+x)(8z^2+zx-x^2)}^{\text{viscous response}} \\ & -2x\sum_{n=1}^{\infty}\frac{1}{\beta_n^4\sin\beta_n}\{(\beta_n\cos(\beta_n z/x)-\beta_n\cos\beta_n)(\tfrac{1}{2}+(\cos\beta_n-1)/\beta_n^2) \\ & -(\beta_n\cos(\beta_n z/x)-\sin\beta_n)(1-\sin\beta_n/\beta_n)\} \\ & \times\Bigg\{\overbrace{\frac{(\beta_n/x)^2\cos(2\pi t)+2\pi\sin(2\pi t)}{(\beta_n/x)^4+(2\pi)^2}}^{\text{inertial response}}\overbrace{-\frac{(\beta_n/x)^2\exp(-(\beta_n/x)^2 t)}{(\beta_n/x)^4+(2\pi)^2}}^{\text{transient response}}\Bigg\}, \end{aligned} \tag{19}$$

where $\beta_n$ are the non-zero positive roots of the equation $\sin\beta_n = \beta_n\cos\beta_n$.

## 4. Discussion of the asymptotic solution

Some of the components of the zero-order velocity (19) have been labelled to identify the physical balance that gives rise to those components. The unlabelled components in the summation term of (19) yield the vertical structure of the velocity. The most important distinction to draw between the various components is between the large-time periodic components and the transient components. Note that the size of the domain is unlimited and so there is no upper bound on $x$. Also, the e-folding time of the transient terms of (19) is

$$t_e = (x/\beta_1)^2 \approx 0.0495x^2. \tag{20}$$

This means that for any finite value of $t$, there will always be a value of $x$ for which the transient terms are significant. However, for a finite $x$, there will be a time after which the transient terms are negligible so it makes sense to refer to the transient and large-time responses. The two regimes will be discussed separately though there are many common features.

### 4.1 *Large-time velocity behaviour*

The large-time periodic behaviour of the velocity $u^{(0)}$ has two components: the 'viscous response' and the 'inertial response'. The viscous response arises from an internal balance between the horizontal pressure gradient and vertical shear. This part of the solution dominates the inertial response as $x \to 0$. This behaviour can be

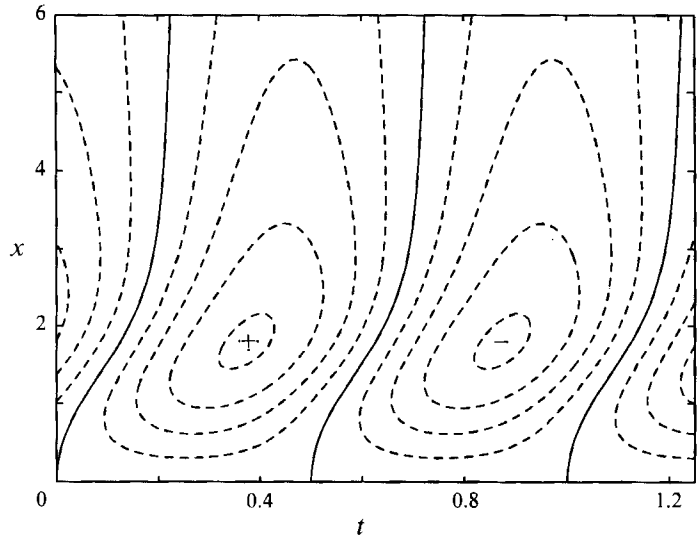


FIGURE 2. Contours of the large-time surface velocity in the $(t, x)$-plane. The solid contour is the zero contour and plots the position of an up/downwelling front that emerges from $x = 0$. The contour interval is $10^{-3}$.

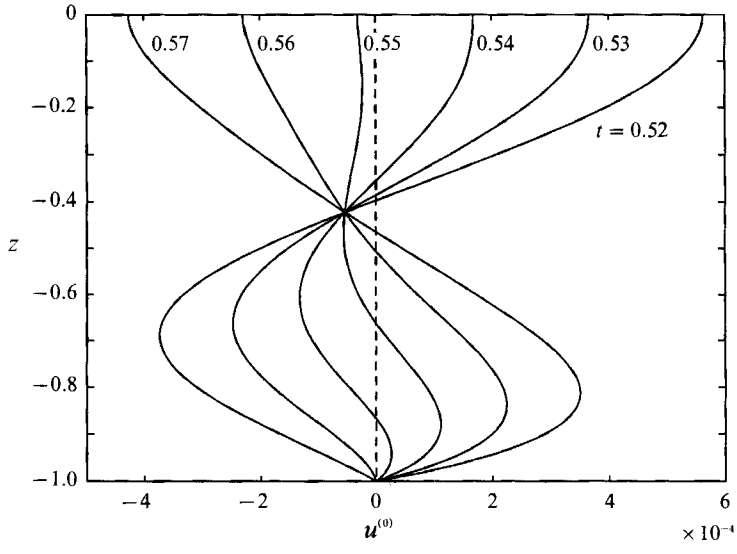


FIGURE 3. Velocity profiles at $x = 1$ near the time that there is a reversal of the flow. The pressure gradient reverses at $t = 0.5$. At $t = 0.54$, a three-layer structure in the flow is evident.

physically explained as follows. As the depth decreases, the time taken for viscosity to act over the local depth decreases, that is, the flow develops more rapidly as $x \to 0$. In the limit as $x \to 0$, $u^{(0)}$ responds instantaneously to changes in the pressure gradient which locks the phase of $u^{(0)}$ to that of the pressure gradient.

The inertial response arises from an internal balance between the inertia of the fluid and the horizontal pressure gradient. Interpretation of this component is complicated by the fact that even though the temporal behaviour of this term is dominated by inertia, the actual velocity profile is governed by vertical shear. For $x \gg 1$, this component dominates the viscous response and lags the pressure gradient by one quarter of a period.

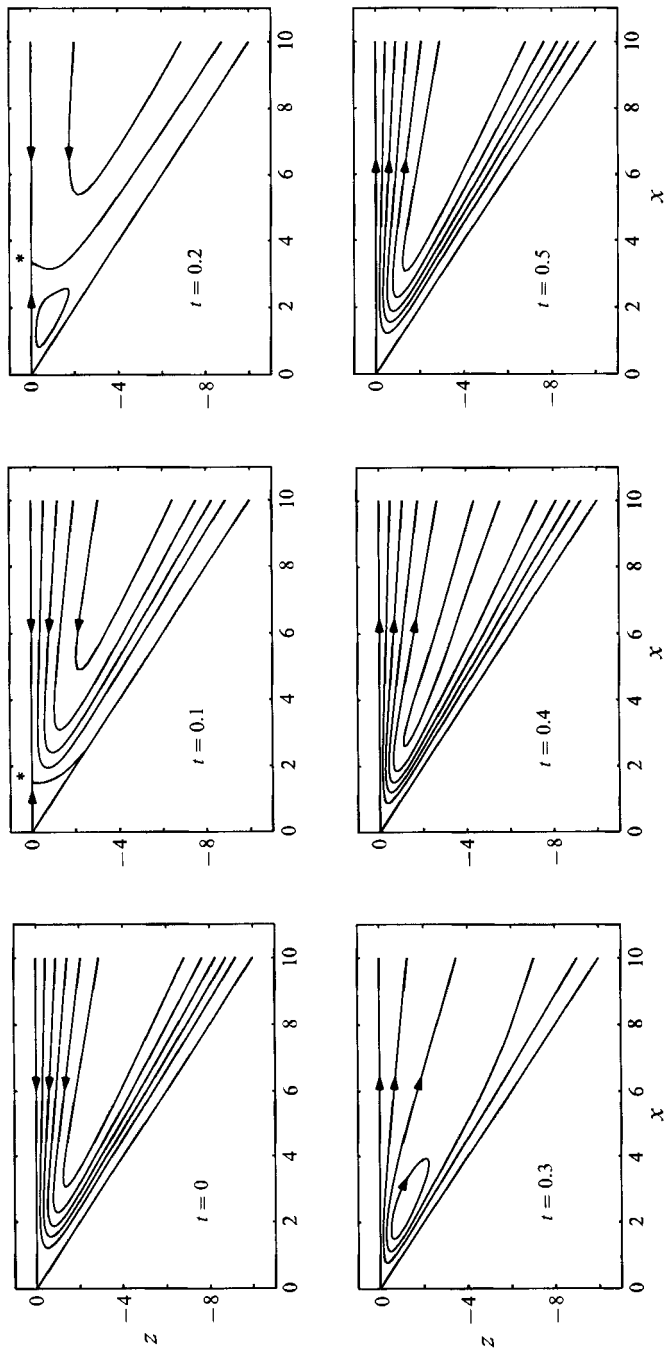


FIGURE 4. Streamlines at various times showing the internal structure of the front as it propagates through the fluid. While the front is present, the flow is divided into two regions circulating in opposite directions. The asterisk denotes the position of zero surface velocity.

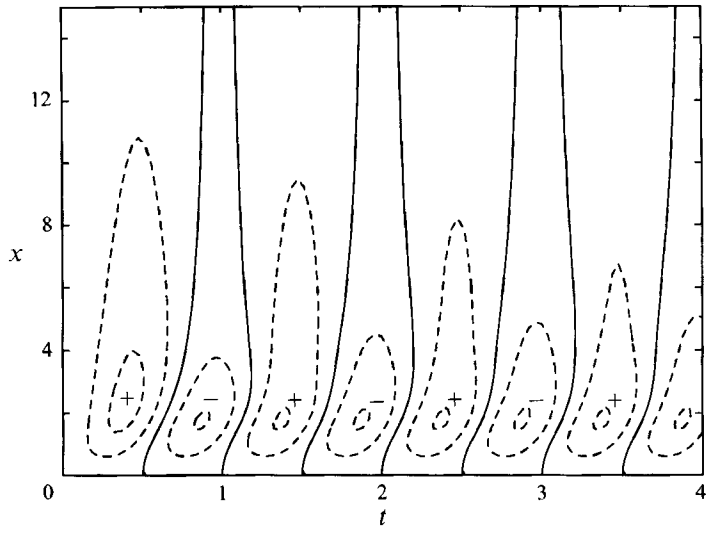


FIGURE 5. Contours of the surface velocity in the $(t,x)$-plane for a few periods of the forcing after its initiation. The solid contour is the zero contour. The contour interval is $2 \times 10^3$.

A summary of the large-time periodic behaviour of the velocity is shown in figure 2. In this figure, contours of the surface velocity $u^{(0)}|_{z=0}$ at large times are shown over one and a quarter periods of the forcing. In this plot, $t = 0$ corresponds to the reversal of the temperature gradient from positive to negative and thus marks the beginning of the daytime circulation pattern. The solid contour is the zero contour and thus represents a point on the surface where the surface velocity changes sign. At this point, the flow is either upwelling or downwelling depending on the sign of the horizontal pressure gradient. If the flow is outwards at the surface near the tip (corresponding to a negative horizontal pressure gradient) then the solid contour plots the position of a downwelling front as it moves out from $x = 0$. The front emerges from $x = 0$ as soon as there is a reversal of the pressure gradient, reflecting the rapid response of the viscous-dominated flow there. As time increases, the front moves outward, slowing briefly near $x = 2$ before moving rapidly off to $x = \infty$ precisely one quarter of a period after it emerged from $x = 0$. After the front has moved off to $x = \infty$ the surface velocity has the same sign everywhere, meaning that the circulation in the sidearm has been completely reversed by the reversed pressure gradient. One quarter of a period after the front has moved off to $x = \infty$, a new front (with the opposite sign) emerges from $x = 0$ and exhibits the same behaviour.

Thus the large-time periodic behaviour of the velocity is characterized by an up/downwelling front emerging from $x = 0$ every time there is a reversal of the horizontal pressure gradient.

Figure 3 shows a series of velocity profiles at $x = 1$ near the time that there is a reversal of the flow. Note that at $t = 0.52$, the velocity profile is very close to the classic cubic profile of Cormack, Stone & Leal (1975) for the flow in a shallow, differentially heated rectangular cavity with a stress-free surface. In fact, the component labelled the 'viscous response' in (19) is identical (up to a multiplicative constant and a coordinate transformation) to that obtained by Cormack *et al.* (1975). The pressure gradient reverses at $t = 0.5$, when an (in this case) upwelling front emerges from $x = 0$. The flow near $z = -1$ is the first to reverse. This is to be expected since the flow near the rigid boundary is dominated by viscous effects

(rather than inertia) and thus will respond more rapidly to the reversal of the pressure gradient. As time increases, the horizontal pressure gradient overcomes the inertia of the fluid and, combined with vertical shear, reverses the entire flow at $t \approx 0.55$. Note that at $t = 0.54$, there is a three-layer velocity structure with outflow both at the surface and near the bottom boundary.

The three-layer structure of the flow can clearly be seen in figure 4 where streamlines are plotted for various times. The internal structure of the front can be deduced from the position of the zero streamline, which is a dividing streamline; this streamline divides the flow into two regions circulating in opposite directions. The front detaches from the sloping bottom $z = -x$ at $t = 0$ and moves into the interior of the domain. The point where the front intersects the surface $z = 0$ corresponds to the propagating fronts discussed previously. At $t = 0.20$, the two regions circulating in opposite directions can be seen clearly. The front continues to move outwards as time progresses, and at $t = 0.25$ the front has moved off to $x = \infty$ and the flow in the sidearm has completely reversed. The flow continues to accelerate with the size of the recirculating region evident at $t = 0.3$ increasing, ultimately encompassing the entire domain.

### 4.2. *Transient velocity behaviour*

The discrepancy in timescales for different values of $x$ leads to an interesting phenomenon in the transient flow that can be seen in figure 5. In this figure, contours of the surface velocity $u^{(0)}|_{z=0}$ are plotted in the $(t, x)$-plane over several periods of the forcing after the forcing is initiated. Thus, $u^{(0)} = 0$ at $t = 0$. The pressure gradient is negative from $t = 0$ to 0.5 and the surface velocity is positive everywhere in this region, indicating that there is a warm surface outflow. At $t = 0.5$, the pressure gradient reverses and a weak upwelling front emerges from $x = 0$ in a similar way to the fronts discussed previously. The front behaves slightly differently however as it moves out more slowly and does not move off to $x = \infty$ until $t = 1.0$ when there is a reversal of the pressure gradient. Thus the front here is present for twice as long as the fronts discussed in the previous section. This is because for $x \gg 1$ and small times, viscosity is barely influencing the flow and the inertia gained by the fluid between $t = 0$ and 0.5 is only just overcome by the pressure gradient between $t = 0.5$ and 1.0. In the limit as $x \to \infty$, vertical shear has no effect on the flow and the flow there will not be reversed. This means that the two zero contours asymptotically approach each other. The fact that there is a change in sign of the surface velocity just before $t = 1.0$ reflects the small effect that viscosity has had up to that time.

Of particular interest here is that shortly after the pressure gradient reverses at $t = 1.0$ and a downwelling front moves out from $x = 0$, a short-lived upwelling front moves in towards the tip from $x = \infty$. The two fronts meet near $x = 3$ at $t = 1.17$ and cancel each other out. After the fronts have met, the circulation in the whole sidearm is in one direction with a warm outflow at the surface. This curious sequence of events is repeated one period later near $t = 2.0$ with some modifications to the behaviour. The downwelling front that emerges from $x = 0$ at $t = 1.5$ moves off to $x = \infty$ more rapidly than the front that appeared shortly after $t = 0.5$. Also, the front that appears from $x = \infty$ emerges a little later in the cycle. This leads to the two fronts meeting further out near $x = 4$. Finally, it takes a little longer for the two fronts to meet, which occurs at $t \approx 2.2$. This change in the behaviour reflects the increasing importance of viscosity for $x > 1$. As time increases, viscosity diffuses the effect of the boundaries into the core region of the flow. Yet another period later, the same sequence of events occurs with similar modifications.

The internal evolution of the two surface fronts is shown in figure 6 where

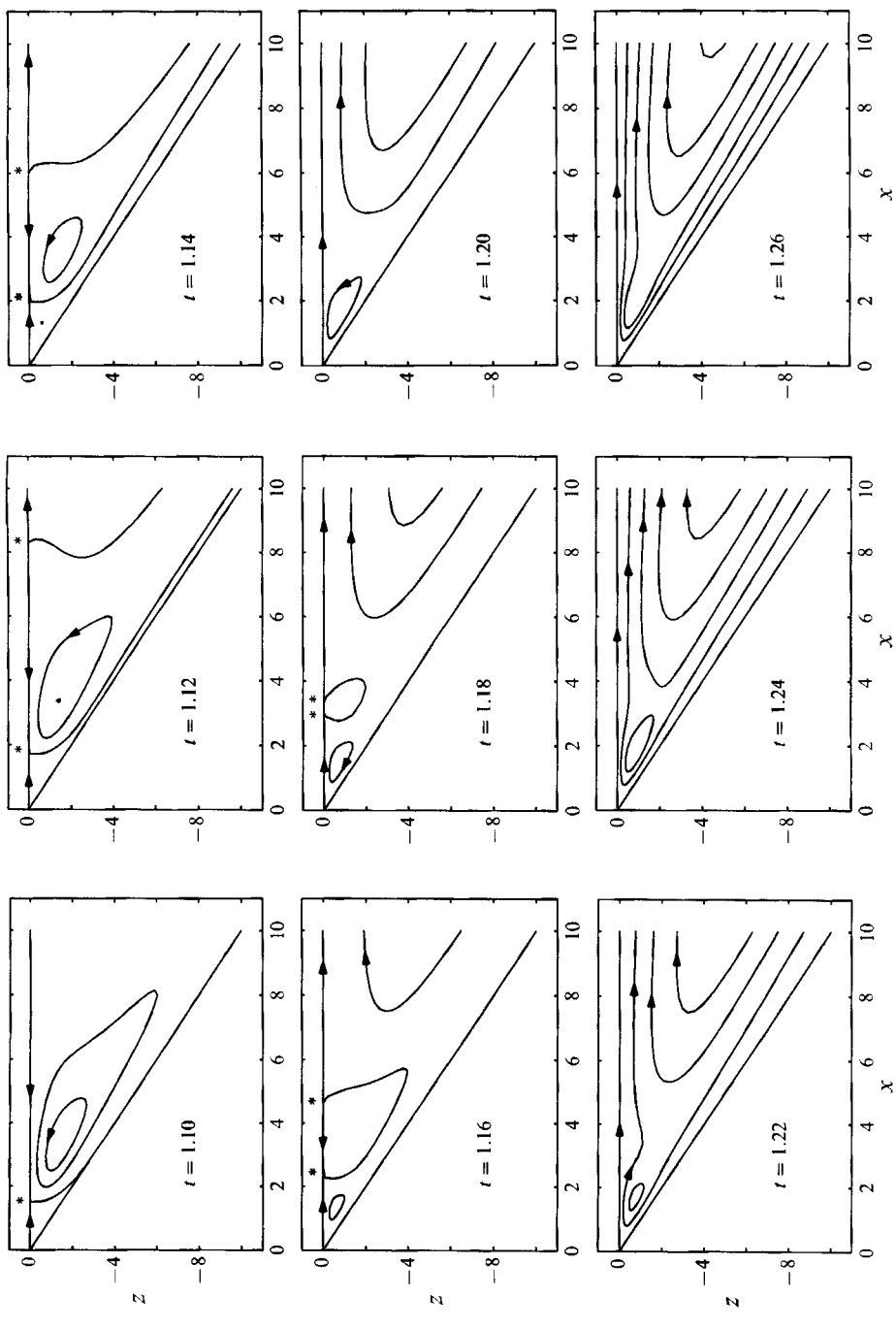


FIGURE 6. Streamlines for various times after the forcing has been initiated. The contour interval is $5 \times 10^{-4}$. The asterisk indicates the position of zero surface velocity.

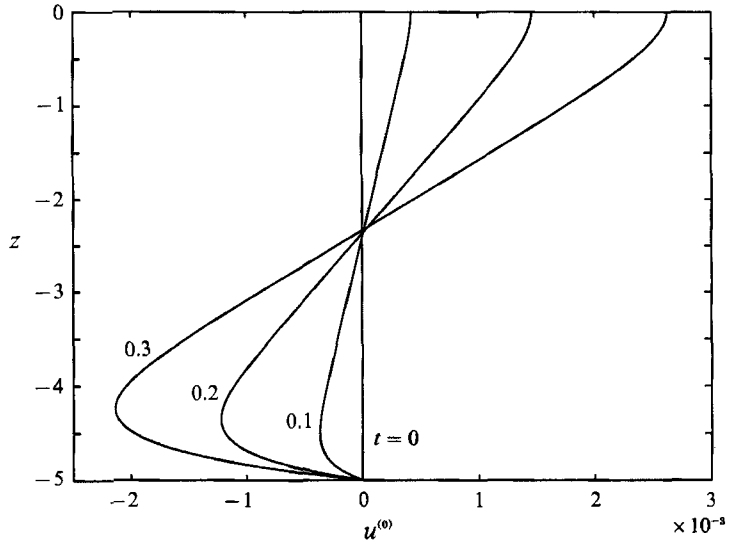


FIGURE 7. Velocity profiles at $x = 5$ for a number of times just after the forcing has been initiated.

streamlines are plotted for various times. The pressure gradient reversed at $t = 1.00$ and in the first plot, at $t = 1.10$, only one front is evident which emerged from $x = 0$ at $t = 1.00$. At $t = 1.12$, the second front that appeared from large $x$ can be seen at the right of the plot. As the two fronts move towards each other, the flow between them is decelerating ($t = 1.12$–$1.14$) while the flow outside this region ($x \ll 1$ and $x \gg 1$) is accelerating. These two regions have different internal balances. For $x \ll 1$, the viscous-dominated flow there is responding rapidly to the increasing pressure gradient. Thus the flow for $x \ll 1$ is accelerating because the pressure gradient is increasing. For $x \gg 1$, even though the flow is dominated by inertia, the pressure gradient does not have much inertia to overcome and has thus reversed rapidly. The flow for $x \gg 1$ is dominated by inertia and thus would accelerate even if the pressure gradient was constant. At $t = 1.16$, the fronts now form a closed streamline within the flow. As time moves on ($t = 1.16$–$1.18$), the size of the closed-off region associated with the closed streamline decreases as does the magnitude of the circulation within it. At the same time, the magnitude of the circulation outside is increasing because of the favourable pressure gradient At $t = 1.20$, the closed zero streamline has vanished altogether and the remaining flow consists of two regions circulating in the same direction. The flow continues to accelerate ($t = 1.20$–$1.26$) and the initially distinct regions of circulating fluid slowly merge.

The internal velocity structure is characterized by an initial balance between inertia and the horizontal pressure gradient. This balance is maintained until viscosity has had sufficient time to diffuse the effect of the boundaries into the core region of the flow. Figure 7 shows a series of velocity profiles at $x = 5$ for various times after the forcing has been initiated. For small times, the flow away from the boundaries is a linear function of $z$ which reflects the fact that the effect of the boundaries has not yet been felt by the core flow and the balance is between the horizontal pressure gradient and inertia.

### 4.3. *Validity of the asymptotic solution*

Because the $O(A^0)$ temperature $T^{(0)}$ is singular at $x = 0$ and hence the horizontal gradient of $T^{(0)}$ is also singular, the range of validity of the asymptotic solution needs to be addressed. It can be shown that $u^{(0)}$ has the following properties:

$$u^{(0)} \propto \begin{cases} 1/x & \text{as} \quad x \to \infty, \\ x & \text{as} \quad x \to 0. \end{cases} \tag{21}$$

Now, the exact temperature equation is

$$\overbrace{\frac{\partial T}{\partial t}}^{O(A^0)} + A^2 Gr\left(u\frac{\partial T}{\partial x} + w\frac{\partial T}{\partial z}\right) = \frac{1}{\sigma}\left(A^2\frac{\partial^2 T}{\partial x^2} + \overbrace{\frac{\partial^2 T}{\partial z^2}}^{O(A^0)}\right) + \overbrace{\cos(2\pi t)/x}^{O(A^0)}, \tag{22}$$

where it has been made explicit which terms are included in the $O(A^0)$ solution. Using the $O(A^0)$ solution yields the following estimates for each of the terms in the above equation:

$$\left.\begin{aligned} \partial T/\partial &\propto 1/x \quad \text{as} \quad x \to 0, \infty, \\ u\,\partial T/\partial x &\propto 1/x \quad \text{as} \quad x \to 0, \\ &\propto 1/x^2 \quad \text{as} \quad x \to \infty, \\ \partial^2 T/\partial x^2 &\propto 1/x^3 \quad \text{as} \quad x \to 0, \infty, \end{aligned}\right\} \tag{23}$$

where the constant of proportionality will actually be a function of time. The remaining terms ($wT_z$ and $T_{zz}$) are identically zero at $O(A^0)$. The asymptotic solution will give a reasonable solution as long as the terms that are not included in the $O(A^0)$ equation are smaller than those that are included. This is certainly the case for sufficiently large $x$. However, as $x \to 0$, the horizontal conduction term $T_{xx}$ is proportional to $1/x^3$, while the terms included in the $O(A^0)$ equation are proportional to $1/x$. This means that no matter how small $A$ is, there will always be some region near the tip where the asymptotic solution will fail. The extent of the region will depend on the value of $A$.

Even though the asymptotic solution fails near $x = 0$, the effect on the solution is relatively minor. The failure arises because the zero-order equation does not include horizontal conduction, which plays a dominating role for small $x$. The effect of horizontal conduction is to reduce the magnitude of the horizontal temperature gradients there. This in turn will lead to a reduction in the associated horizontal velocity. Thus, the failure of the asymptotic solution in the tip will lead to an overestimation of the velocities there. Again, the amount that the velocities are overestimated by will depend on the value of $A$.

## 5. Numerical simulation

The asymptotic solutions of this paper are only valid for $A \ll 1$ and moderate $Gr$ and do not provide insight into higher-order effects such as advection. The numerical simulation that will be described in this paper has two aims. The first is to validate the $O(A^0)$ solutions found earlier in this paper and the second is to provide some insight into higher-order, particularly nonlinear, behaviour.

Owing to the difficulty of finding exact solutions for general natural convection problems, there is a large body of literature devoted to numerically modelling convective flows. A recent review of numerical methods applicable to convective

flows can be found in Patankar (1988). The method used in this paper is adapted from a method described by Armfield (1991) which includes a survey of more recent numerical schemes.

The wedge-shaped geometry of the flow domain suggests formulating the problem in polar coordinates. For the analytical problem considered in §§2–4, there is no advantage in using polar coordinates. However there are considerable numerical advantages associated with having the boundaries of the flow domain lying on coordinate lines. The equations of motion become, after using the non-dimensionalization scheme described above with $r$ and $\theta$ scaling with $A^{-1}(\nu P)^{\frac{1}{2}}$ and $A$ respectively,

$$\frac{\partial u}{\partial t}+A^2Gr\left(u\frac{\partial u}{\partial r}+\frac{1}{r}w\frac{\partial u}{\partial \theta}\right)-A^4Gr\frac{1}{r}w^2=-\frac{\partial p}{\partial r}$$
$$+A^2\frac{1}{r}\frac{\partial}{\partial r}\left(r\frac{\partial u}{\partial r}\right)+\frac{1}{r^2}\frac{\partial^2 u}{\partial \theta^2}-A^2\frac{2}{r^2}\frac{\partial w}{\partial \theta}-A^2\frac{1}{r^2}u+\frac{1}{A}T\sin A(\theta-1), \quad (24)$$

$$\frac{\partial w}{\partial t}+A^2Gr\left(u\frac{\partial w}{\partial r}+\frac{1}{r}w\frac{\partial w}{\partial \theta}+\frac{1}{r}wu\right)=-\frac{1}{rA^2}\frac{\partial p}{\partial \theta}$$
$$+A^2\frac{1}{r}\frac{\partial}{\partial r}\left(r\frac{\partial w}{\partial r}\right)+\frac{1}{r^2}\frac{\partial^2 w}{\partial \theta^2}+\frac{2}{r^2}\frac{\partial u}{\partial \theta}-A^2\frac{1}{r^2}w+\frac{1}{A^2}T\cos A(\theta-1), \quad (25)$$

$$\frac{\partial T}{\partial t}+A^2Gr\left(u\frac{\partial T}{\partial r}+\frac{1}{r}w\frac{\partial T}{\partial \theta}\right)=\frac{1}{\sigma}\left(A^2\frac{1}{r}\frac{\partial}{\partial r}\left(r\frac{\partial T}{\partial r}\right)+\frac{1}{r^2}\frac{\partial^2 T}{\partial \theta^2}\right)+\frac{\cos(2\pi t)}{r\cos(A(\theta-1))}, \quad (26)$$

$$\frac{1}{r}\frac{\partial}{\partial r}(ru)+\frac{1}{r}\frac{\partial w}{\partial \theta}=0, \quad (27)$$

where all quantities are non-dimensional, $r$ is the radial coordinate, $\theta$ is the angle measured anticlockwise from the bottom boundary, $u$ is the radial velocity, $w$ is the tangential velocity, $p$ is pressure, $T$ is the temperature and $Gr$ is defined by (6). The solution domain is now $r_{\min} < r < r_{\max}$ and $0 < \theta < 1$. The upper limit on $r$ must be chosen so that there is a significant part of the flow not affected by the presence of the endwall at $r = r_{\max}$ which is absent for the asymptotic solutions found in §4. Setting $r_{\max} = 10$ is sufficient to ensure that there is a substantial region of the flow not affected by the endwall whilst ensuring that the domain does not become too large to be feasibly simulated. At the tip, $r_{\min}$ is chosen so that it lies within the conduction-dominated regime where the velocities are small. Setting $r_{\min} = 0.1$ is sufficient to ensure that the boundary there does not have a significant effect on the temperature and flow dynamics.

The primary aim here is to compare the numerical and asymptotic solutions. However, the numerical model is restricted to a finite domain while the model formulated in §2 is not. Also, the numerical model includes a boundary at $r = r_{\min} > 0$ which is absent in the analytical model. Thus there are extra boundary conditions that need to be formulated besides those that arise naturally from the analytical model.

The heat flow in the tip region is dominated by conduction, thus the boundary condition chosen here for the temperature is simply that the temperature gradient at $r = r_{\min}$ matches that of the asymptotic solution, that is

$$\frac{\partial T}{\partial r}=-\frac{\sin(2\pi t)}{2\pi r^2\cos A(\theta-1)} \quad \text{on} \quad r=r_{\min}. \quad (28)$$

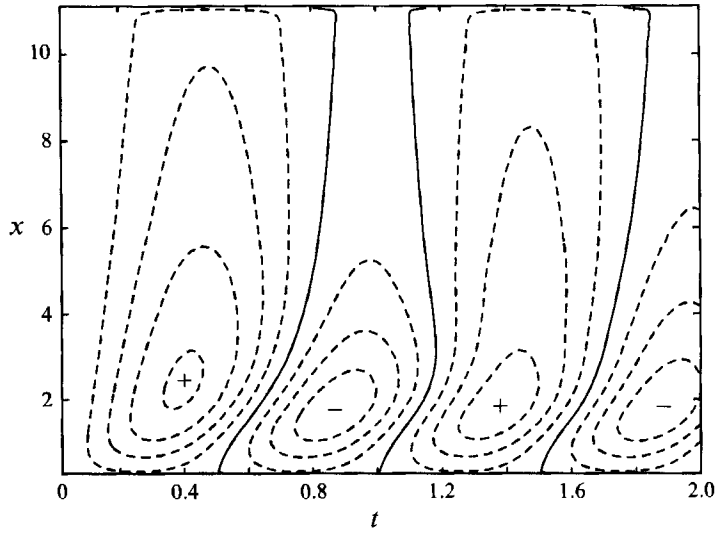


FIGURE 8. Contour plot of the numerically calculated surface velocity in the $(t, x)$-plane with $A = 0.02$, $Gr = 5 \times 10^4$ and $\sigma = 7.5$. The contour interval is $10^{-3}$.

The position of the boundary at $r = r_{\max}$ is chosen so that it has a small influence on the velocity and temperature fields in the bulk of the sidearm. For simplicity, the boundary condition here for the temperature is

$$\partial T/\partial r = 0 \quad \text{on} \quad r = r_{\max}. \tag{29}$$

The boundaries at $r = r_{\min}$ and $r = r_{\max}$ are assumed to be solid, leading to the velocity boundary conditions

$$\left.\begin{aligned} u = w = 0 \quad &\text{on} \quad r = r_{\min}, \\ u = w = 0 \quad &\text{on} \quad r = r_{\max}. \end{aligned}\right\} \tag{30}$$

The boundary conditions on the remaining boundaries follow from §2 and are

$$\left.\begin{aligned} \partial T/\partial\theta = \partial u/\partial\theta = w = 0 \quad &\text{on} \quad \theta = 1, \\ \partial T/\partial\theta = u = w = 0 \quad &\text{on} \quad \theta = 0. \end{aligned}\right\} \tag{31}$$

The scheme used for numerically simulating the above system of equations is a modified version of a scheme developed by Armfield (1991). Essentially, the method is a SIMPLE type scheme applied on a non-staggered grid with QUICK correction for the convective terms. A detailed description of the SIMPLE scheme and some of the early modifications can be found in Patankar (1980). The approximate pressure equation is formulated so that the scheme is elliptic (Armfield 1991). The computational domain is discretized used a $41 \times 33$ non-uniform grid. A small time step of $10^{-4}$ is required to resolve the rapid flow development in the tip.

### 5.1 *Results and discussion*

The simulation reported here is for the transient part of the flow as computational restraints did not allow the simulation to run to the large-time periodic behaviour discussed in §4.1. Thus, this simulation is restricted to two periods of the forcing after it has been initiated. The values of the non-dimensional parameters used for this simulation are $A = 0.02$, $\sigma = 7.5$ and $Gr = 5 \times 10^4$. For these values of the non-dimensional parameters and using the $O(A^0)$ solution to estimate the size of $u$, the ratio of the unsteady inertia term to the horizontal advection term in the radial momentum equation is approximately 10. This suggests that for these values of the

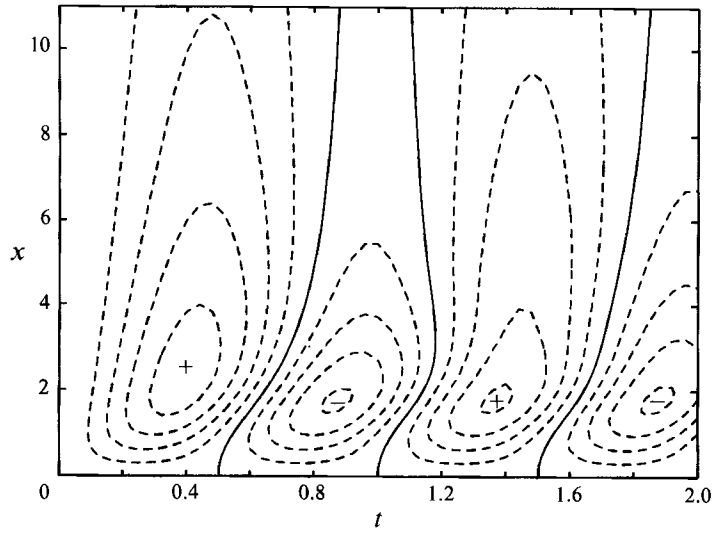


FIGURE 9. Contour plot of the asymptotic surface velocity in the $(t, x)$-plane. The contour interval is $10^{-3}$.

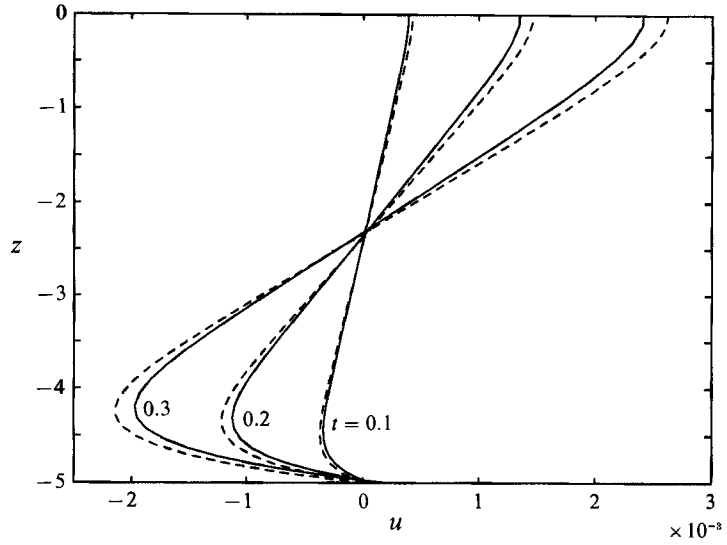


FIGURE 10. Comparison between the numerical (solid lines) and asymptotic (dashed lines) velocity profiles at $x = 5$ for various times including the initial inertia-dominated regime.

non-dimensional parameters, nonlinear effects are small, but not negligible, and so this simulation provides an opportunity to validate the asymptotic solutions found in §4 and to examine the effect that a small amount of advection has on the dynamics, and is also close to the value for $GrA^2$ above which the asymptotic solutions fail. As before, the time-dependent behaviour is summarized by a contour plot of the surface velocity in the $(t, x)$-plane. Figure 8 shows such a plot using data from the simulation. Figure 9 shows the corresponding plot using the asymptotic solution. Within the interior of the computational domain, the agreement between the two plots is quite good. The numerical velocities are slightly smaller than the analytical solution as can be seen in figure 10. This is due to the small effect that horizontal diffusion has had on the temperature field. This overestimation of the

velocities by the asymptotic solution was discussed in §4 and is due to the absence of horizontal conduction of heat in the $O(A^0)$ equations. Another less significant effect that contributes to the difference is horizontal advection. Even though the nonlinear effects are small, advection of heat reduces the size of the horizontal pressure gradient slightly. There is some discrepancy between the results near $x = 11$ where the solid boundary that is absent in the asymptotic solutions is influencing the flow. The effect of the boundary at $x = 11$ is restricted to $O(A)$ of the domain. Of particular interest is the position and time of appearance of the up/downwelling fronts discussed in §5 about which the numerical and asymptotic solutions are in excellent agreement.

Figure 10 shows a comparison between the numerical and asymptotic solutions for the velocity profiles at various times at $x = 5$. Again, there is good agreement between the two solutions with the asymptotic velocities being slightly larger. The values of $x$ and $t$ chosen include the initial inertial regime where the profiles are nearly linear as well as the later viscous regime where the profiles are closer to cubic.

## 6. Concluding remarks

The model proposed and asymptotically solved in this paper is a limited representation of the true geophysical situation. Despite this, a comparison between the results of this paper and available field data is useful. The dimensional velocity in this paper is given by

$$u' = \frac{Ag\alpha I_0 P^2}{\rho_0 C_p (\nu P)^{\frac{1}{2}}} u. \tag{32}$$

Using the parameter values $I_0 = 10^3\,\mathrm{Wm}^2$ and $A = 0.02$ from Monismith *et al.* (1990) and the usual values for the other parameters yields a velocity of $5\ \mathrm{cm\ s}^{-1}$ for a typical value of $\nu$ of $10^{-4}\ \mathrm{m\ s}^{-2}$. The drogue measurements of Monismith *et al.* yielded a peak velocity of $7.5\ \mathrm{cm\ s}^{-1}$ while the measurements of Adams & Wells (1984) yielded velocities up to $15\ \mathrm{cm\ s}^{-1}$. Thus, the magnitude of the velocities predicted by this model are consistent with those measured in the field. Monismith *et al.* observe that the lag between a reversal of the forcing and a reversal of the flow within a sidearm can be longer than the 6 hours suggested by the large-time response considered in §4.1. However the discussion in §4.2 shows that even when the forcing is periodic, the lag can be up to 12 hours if the transient effects are taken into account. In particular, if the magnitude of the, say, daytime forcing is less than that of the previous night's forcing then it will take longer for the weaker forcing to overcome the night-time flow. Thus it would appear that the model considered in this paper has captured much of the bulk flow dynamics of a periodically forced reservoir sidearm.

The authors are grateful to Greg Ivey, Kreshimir Zic and the anonymous reviewers for valuable comments on earlier drafts of this paper. This research was carried out while one of us (D.F.) was a recipient of an Australian Postgraduate Research Award along with a Centre for Water Research Scholarship.

## REFERENCES

ADAMS, E. E. & WELLS, S. A. 1984 Field measurements on side arms of Lake Anna, Va. *J. Hydraul. Engng* **110**, 773–793.

ARMFIELD, S. W. 1991 Finite-difference solutions of the Navier–Stokes equations on staggered and non-staggered grids. *Computers Fluids* **20**, 1–17

BROCARD, D. N. & HARLEMAN, D. R. F. 1980 Two-layer model for shallow convective circulation. *J. Fluid Mech.* **100**, 129–156.

CORMACK, D. E., LEAL, L. G. & IMBERGER, J. 1974 Natural convection in a shallow cavity with differentially heated end walls. Part 1. Asymptotic theory. *J. Fluid Mech.* **65**, 209–229.

CORMACK, D. E., STONE, G. P. & LEAL, L. G. 1975 The effect of upper surface conditions on convection in a shallow cavity with differentially heated end-walls. *Intl J. Heat Mass Transfer* **18**, 635–648.

HORSCH, G. M. & STEFAN, H. G. 1988 Convective circulation in littoral water due to surface cooling. *Limnol. Oceanogr.* **33**, 1068–1083.

IMBERGER, J. & PATTERSON, J. C. 1990 Physical limnology. *Adv. Appl. Mech.* **27**, 303–475.

JAIN, S. C. 1982 Buoyancy-driven circulation in free-surface channels. *J. Fluid Mech.* **122**, 1–12.

KIRK, J. T. O. 1986 Optical limnology – a manifesto. In *Limnology in Australia* (ed. P. de Dekker & W. D. Williams), pp. 33–62. CSIRO Publications Sales.

MONISMITH, S. G., IMBERGER, J. & MORISON, M. L. 1990 Convective motions in the sidearm of a small reservoir. *Limnol. Oceanogr.* **35**, 1676–1702.

PATANKAR, S. V. 1980 *Numerical Heat Transfer and Fluid Flow.* Hemisphere.

PATANKAR, S. V. 1988 Recent developments in computational heat transfer. *Trans. ASME* C: *J. Heat Transfer* **110**, 1037–1045.

PATTERSON, J. C. 1984 Unsteady natural convection in a cavity with internal heating and cooling. *J. Fluid Mech.* **140**, 135–151.

PATTERSON, J. C. 1987 A model for convective motions in reservoir sidearm. In *Proc. XXII Congress IAHR, Laussane, 1987*, pp. 68–73.

POULIKAKOS, D. & BEJAN, A. 1983 The fluid mechanics of an attic space. *J. Fluid Mech.* **131**, 251–269.

SCOTT, C. F. 1988 On the circulation and classification of shallow estuaries. Ph.D. thesis, Western Australia.

SCOTT, C. F. & IMBERGER, J. 1988 Three-dimensional estuary circulation and classification. In *Proc. Intl Conf. Physics of Shallow Estuaries and Bays* (ed. R. Cheng). Springer.

STURM, T. W. 1981 Laminar convection of heat in dead-end channels. *J. Fluid Mech.* **110**, 99–114.